$3\,^1\Pi_u$ and $3\,^1\Sigma_u^+$ states of K_2 studied by a polarization-labeling spectroscopy technique

W. Jastrzębski[1] and P. Kowalczyk[2]
[1]*Institute of Physics, Polish Academy of Sciences, aleja Lotników 32/46, 02-668 Warsaw, Poland*
and [2]*Institute of Experimental Physics, Warsaw University, ulica Hoża 69, 00-681 Warsaw, Poland*
(Received 15 June 1994)

The $3\,^1\Pi_u \leftarrow X\,^1\Sigma_g^+$ and $3\,^1\Sigma_u^+ \leftarrow X\,^1\Sigma_g^+$ band systems of K_2 are studied by the polarization-labeling spectroscopy method. An observation of isotope shifts of rotationally resolved lines in both systems reveals that the previous vibrational numbering in the $3\,^1\Pi_u$ and $3\,^1\Sigma_u^+$ states is incorrect by 1 and 3 vibrational quanta, respectively. An analysis is carried out for both states. We present the resulting molecular parameters that describe the $3\,^1\Pi_u$ state to 55% and the $3\,^1\Sigma_u^+$ state to 71% of their potential well depths.

PACS number(s): 33.20.Kf, 33.15.Fm, 33.15.Mt

I. INTRODUCTION

The diatomic alkali-metal molecules, with their simple electronic configuration and with the main absorption bands conveniently positioned in the visible region, are relatively easy to handle both theoretically and experimentally. Hence they have long been employed for testing quantum chemistry calculations. Modern theoretical methods have the potential to predict potential curves and spectroscopic constants with high accuracy [1]. On the experimental side a huge body of data has been gathered on Li_2 [2] and Na_2 [3] molecules. Less is known about the potassium dimer [4]. In particular, the excited ungerade states lying more than 23 000 cm^{-1} above the bottom of the ground $X\,^1\Sigma_g^+$ state potential have escaped detection until recently.

In our previous work, using the polarization-labeling spectroscopy technique we have been able to observe and analyze the $3\,^1\Pi_u$ and $3\,^1\Sigma_u^+$ states of K_2 in the 23 800–25 600 cm^{-1} region [5]. Molecular constants were derived for the investigated states. However, the vibrational numbering in both states was ambiguous. The unfavorable Franck-Condon factors for the transitions from the ground $X\,^1\Sigma_g^+$ state prevented direct observation of the lowest vibrational levels in $3\,^1\Pi_u$ and $3\,^1\Sigma_u^+$. Thus the vibrational numbering was based solely on comparison of the observed line intensities with patterns of Franck-Condon intensities calculated for various assumed numberings. The results were uncertain at least by one vibrational quantum.

The present paper contains some substantial refinements of the previous study on the $3\,^1\Pi_u$ and $3\,^1\Sigma_u^+$ states of K_2.

(i) The isotope shift between lines of the $^{39}K_2$ and $^{39}K^{41}K$ isotopomers is employed to establish the correct vibrational numbering in both states. The numbering in the $3\,^1\Pi_u$ state is changed by one unit and in the $3\,^1\Sigma_u^+$ state by three units. This influences the values of molecular constants of the states under consideration.

(ii) In addition to the He-Ne laser, the Kr^+ laser is also used for polarization labeling. As a result we increased the number of vibrational progressions investigated and extended the range of rotational quantum numbers J of levels used in the fits of molecular constants.

(iii) Improved sensitivity of the detection system allowed us to observe vibrational levels up to $v'=53$ for the $3\,^1\Pi_u$ state and $v'=36$ for the $3\,^1\Sigma_u^+$ state. Thus we have spectroscopically determined potentials of both states up to more than half of the well depths.

(iv) In the present experiment tuning of the dye laser is controlled with a Fabry-Pérot interferometer. Higher precision in measurement of line positions has improved determination of molecular parameters.

In the following sections we present details of the experimental method and the results of the measurements.

II. EXPERIMENTAL

The basic principle of the V-type optical double-resonance polarization spectroscopy and its experimental realization are schematically depicted in Fig. 1. The two laser beams pass collinearly through a molecular sample, which is placed between crossed polarizers. Contrary to the classical scheme [6,7], in our experiment the probe laser is of fixed frequency whereas the pump laser is tunable. The frequency of the probe laser accidentially coincides with a set of known transitions $B\,^1\Pi_u(v_2',J_2') \leftarrow X\,^1\Sigma_g^+(v_1'',J_1'')$, thus labeling the involved rovibrational levels (v_1'',J_1'') in the ground state of the potassium dimer. The circularly or linearly polarized pump laser light is tuned across the investigated band systems $3\,^1\Pi_u \leftarrow X\,^1\Sigma_g^+$ and $3\,^1\Sigma_u^+ \leftarrow X\,^1\Sigma_g^+$. It orients or aligns the absorbing molecules in the lower (and upper) levels by optical pumping. A linearly polarized weak probe beam is changed in its polarization characteristics whenever the frequency of the pump laser is tuned to a transition originating from the labeled lower level (v_1'',J_1''). The photomultiplier placed behind the crossed analyzer therefore receives a signal at any time the pump laser frequency coincides with a transition

$$3\,^1\Pi_u / 3\,^1\Sigma_u^+(v_3',J_3') \leftarrow X\,^1\Sigma_g^+(v_1'',J_1'') .$$

In the experimental realization of the described method, the pump laser was a pulsed dye laser and XeCl

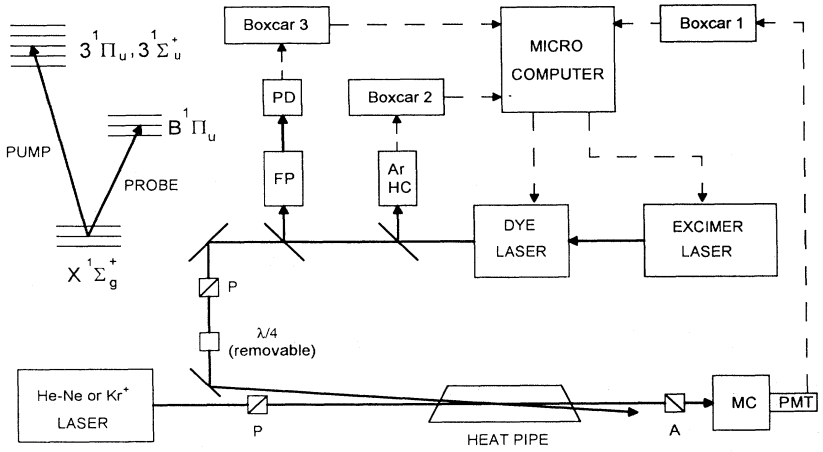

FIG. 1. Excitation scheme and block diagram of the experimental setup: *A*, analyzer; FP, Fabry-Pérot interferometer; HC, hollow-cathode lamp; λ/4, quarter-wave plate; MC, monochromator; *P*, polarizer, PD; photodiode; and PMT, photomultiplier tube. The boxcar integrators are model SR250.

excimer laser system (Lumonics HD500 and EX500). The dye laser was operated in the spectral range 380–429 nm with POPOP, PBBO, and BBQ as laser dyes, providing an output of approximately 2 mJ per pulse and a linewidth less than 0.1 cm^{-1}. Laser frequency was determined absolutely from the optogalvanic spectrum of argon [8] and additionally calibrated by sending part of the laser beam through a 0.5-cm-long Fabry-Pérot interferometer with a free spectral range of 30 GHz. The accuracy in absolute determination of wave numbers over the whole investigated range was better than 0.1 cm^{-1}. For generation of probe light we used two different cw lasers: He-Ne (λ=632.8 nm) or Kr^+ (λ=647.1 nm) with a typical power of 30–50 mW. Table I presents a summary of all the identified labeling transitions induced by the probe lasers, which give rise to the polarization spectra.

The potassium vapor was generated by heating metallic potassium in a heat-pipe oven equipped with fused silica windows of particularly low birefringence. The residual birefringence was additionally compensated by squeezing the windows with adjustable screws. The oven was operated at 590 K with 4 Torr of helium as a buffer gas. Under these conditions the pressures of K and K_2 were 6×10^{-1} Torr and 3×10^{-3} Torr, respectively [9]. Thus the oven did not operate as a true heat pipe but instead contained a mixture of potassium and helium in the central region.

TABLE I. Observed transitions in the $B\,^1\Pi_u \leftarrow X\,^1\Sigma_g^+$ band system of K_2 excited by the fixed-frequency probe lasers. The asterisks indicate excitation of both $^{39}K_2$ and $^{39}K^{41}K$; otherwise only $^{39}K_2$ was excited.

Laser line	Labeled transition $B\,^1\Pi_u(v',J')$-$X\,^1\Sigma_g^+(v'',J'')$
He-Ne, 632.8 nm	(6,18)-(0.19)
	(7,82)-(0,83)
	(8,73)-(1,73)
	(9,55)-(2,55)
	(12,70)-(4,70)
	(13,46)-(5,47)
Kr^+, 647.1 nm	(2,82)-(0,83)*
	(2,95)-(0,94)*

The pump and probe laser beams crossed in the potassium vapor zone at an angle of 10 mrad giving an interaction length of ca. 20 cm. After passing through the analyzer the probe beam was directed to a 0.3-m monochromator centered at the probe laser wavelength and onto the photomultiplier tube with S-20 photocathode. The photoelectric current was averaged with a boxcar integrator (Stanford Research Systems, SR250) and fed to a microcomputer interface (SR245) together with the optogalvanic spectrum of argon and the Fabry-Pérot frequency marks. Apart from data acquisition, the computer was used to trigger the excimer laser and to control tuning of the dye laser.

III. RESULTS AND ANALYSIS

In the present experiment, a total of 636 transitions were assigned to the $3\,^1\Pi_u \leftarrow X\,^1\Sigma_g^+$ system, spanning the range $0 \le v' \le 53$, and 308 transitions to the $3\,^1\Sigma_u^+ \leftarrow X\,^1\Sigma_g^+$ system ($1 \le v' \le 36$). A typical segment of the polarization spectrum is shown in Fig. 2. From the general principles of polarization spectroscopy [6,7] it can be found that when the pump is circularly polarized, only transitions originating from the levels labeled via *P* or *R* lines show up in the polarization spectra, which consist of series of *P*,*R* doublets. The linearly polarized pump beam leads to a richer spectrum. It is dominated by transitions starting from the levels labeled via *Q* lines, but those labeled via *P* or *R* lines also appear weakly. Moreover, the polarization spectra consist of series of *P*,*Q*,*R* triplets (with *Q* lines most intense) in the case of $^1\Pi_u \leftarrow X\,^1\Sigma_g^+$ bands, but only series of *P*,*R* doublets are present for $^1\Sigma_u^+ \leftarrow X\,^1\Sigma_g^+$ bands. Thus the symmetry of the upper state can be easily determined from the structure of the polarization spectrum. The detailed selection rules relevant to our version of the polarization-labeling spectroscopy method will be discussed elsewhere [10].

The measured line positions in both band systems were fitted to differences of term values $\nu = T(v',J')$

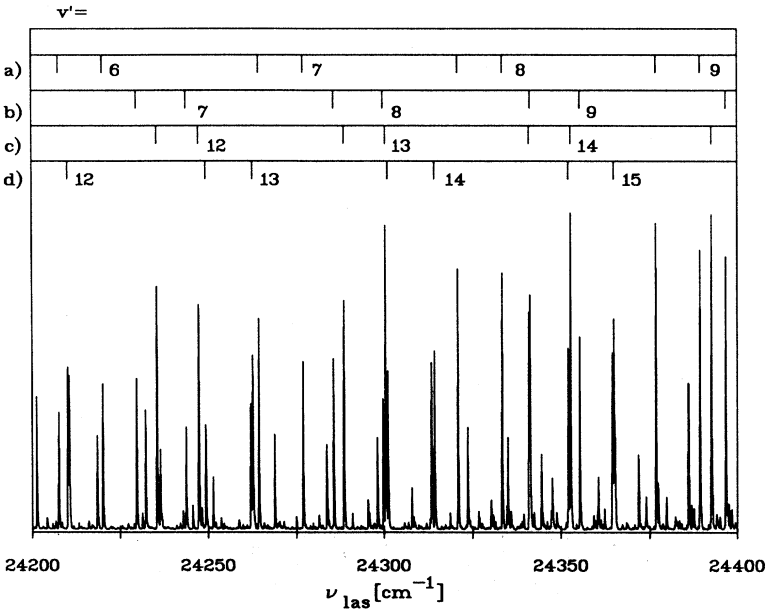

FIG. 2. Segment of the polarization spectrum of K_2 obtained with a Kr^+ laser as the probe laser and a circularly polarized pump beam. The assigned vibrational progressions correspond to the transitions $3\,^1\Pi_u \leftarrow X\,^1\Sigma_g^+$ [(a),(b)] and $3\,^1\Sigma_u^+ \leftarrow X\,^1\Sigma_g^+$ [(c),(d)] from the ground-state levels labeled by the probe laser: $v''=0$, $J''=83$ [(a) and (c)] and $v''=0$, $J''=94$ [(b) and (d)].

$-T(v'',J'')$ of upper and lower levels, which are expressed by the Dunham expansion [11]

$$T(v,J)=T_e+\sum_{i,k}(Y_{ik}+\delta y_{ik})(v+0.5)^i[J(J+1)-\Lambda^2]^k .$$

The δy_{ik} constants describe the Λ doubling in the electronic Π state: $\delta=0$ or 1 for f or e levels, respectively. Since the Dunham coefficients Y_{ik} of the $X\,^1\Sigma_g^+$ ground state are known with high precision [12], they were treated as fixed constants in the subsequent fits. Apart from the spectral lines observed in the present experiment, 52 lines from the bandhead of the (20,0) transition studied under high resolution in the molecular-beam experiment [13,14] have been incorporated in the analysis. Preliminary fits showed that some local perturbations of the $3\,^1\Pi_u$ and $3\,^1\Sigma_u^+$ states had to be taken into account. In the final least-squares fits we omitted all lines for which the difference between the measured and the calculated positions exceeded three times the accuracy of the measurements (i.e., 3×0.1 cm^{-1}). Thus 6% of the measured lines for the $3\,^1\Pi_u$ state and 8% for the $3\,^1\Sigma_u^+$ state were removed. In this manner we suppressed most of the perturbed lines and obtained meaningful sets of Dunham coefficients for both states under consideration. The range of vibrational and rotational levels covered in the final fits is shown in Figs. 3(a) and 3(b).

It is tempting to speculate about the nature of the perturbing states, even if experimental information on them is very limited. Our observations suggested local perturbations of both $3\,^1\Pi_u$ and $3\,^1\Sigma_u^+$ states: removal of a few

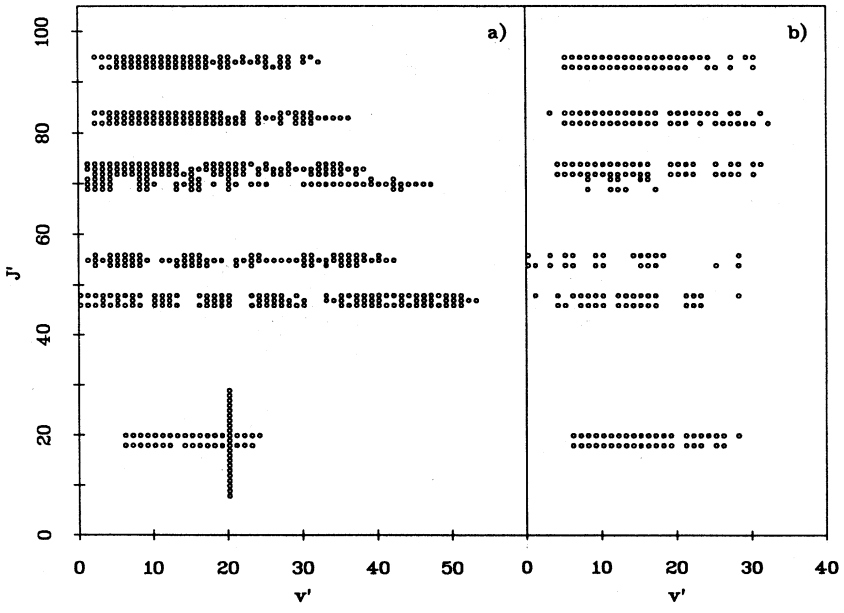

FIG. 3. Distribution of the data used to fit the Dunham coefficients in the field of vibrational and rotational quantum numbers of the $3\,^1\Pi_u$ state (a) and the $3\,^1\Sigma_u^+$ state (b) in K_2.

perturbed rotational lines from the spectra sufficed to restore the regular pattern in them. This is consistent with a weak perturbation of the observed states by some states from the triplet manifold. However, the precise assignment of the perturbers requires an additional study specifically oriented to this problem.

The long vibrational progressions observed in our experiment indicate a big difference between the potential curves of the ground state and both excited states. Indeed, the equilibrium distances as well as vibrational constants of the $3\,^1\Pi_u$ and $3\,^1\Sigma_u^+$ states differ by more than 20% from the corresponding characteristics of the ground state. Under such circumstances transitions to the low levels of the investigated excited states may be strong only when they originate from high v'' levels of the X state. Unfortunately, such levels were not labeled in our experiment. Furthermore, the transitions in question are overlapped by lines of the $C\,^1\Pi_u \leftarrow X\,^1\Sigma_g^+$ and $2\,^1\Sigma_u^+ \leftarrow X\,^1\Sigma_g^+$ band systems [14,15]. Hence the vibrational numbering in the $3\,^1\Pi_u$ and $3\,^1\Sigma_u^+$ states could not be obtained simply by assuming that the longest-wavelength lines in the observed progressions correspond to $v'=0$. In the previous report [5] we attempted to determine the vibrational numbering from a comparison of intensity distributions with estimated Franck-Condon factors. The results were evidently uncertain. In the present work, in addition to the rich spectrum of $^{39}K_2$, we succeeded in observing 97 lines assigned to the $3\,^1\Pi_u \leftarrow X\,^1\Sigma_g^+$ and $3\,^1\Sigma_u^+ \leftarrow X\,^1\Sigma_g^+$ systems in the $^{39}K^{41}K$ isotopomer (see Fig. 4). The observed isotope shifts of the lines provided unambiguous vibrational numbering in both $3\,^1\Pi_u$ and $3\,^1\Sigma_u^+$ states: the assignment given in Ref. [5] proved to be in error by 1 and 3 vibrational quanta, respectively.

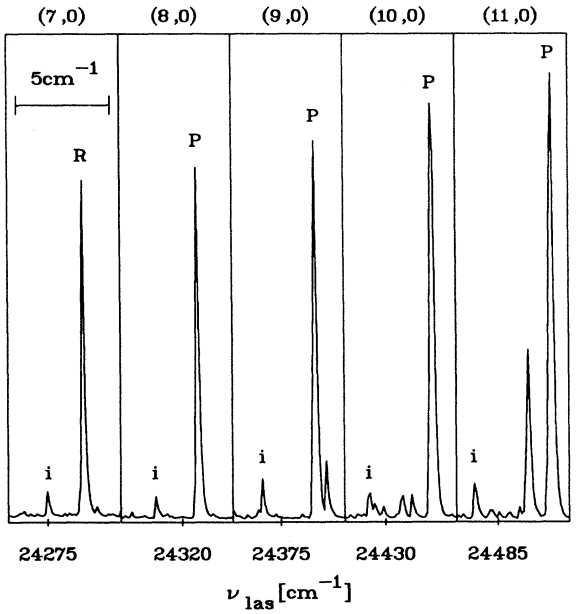

FIG. 4. Details of the polarization spectrum observed at the same conditions as for Fig. 2. The probe laser labels the $v''=0$, $J''=83$ level in both $^{39}K_2$ and $^{39}K^{41}K$. Several lines assigned to transitions originating from this level in the $3\,^1\Pi_u \leftarrow X\,^1\Sigma_g^+$ system are shown. P or R denotes the $P(83)$ or $R(83)$ line in the $^{39}K_2$ molecule; i is the corresponding line in the $^{39}K^{41}K$ isotopomer.

Tables II and III present final sets of Dunham coefficients for the $3\,^1\Pi_u$ and $3\,^1\Sigma_u^+$ states together with their standard errors. The large number of figures (more than are statistically significant) is required for the reproduction of line frequencies to within the error of measurements. According to the discussion in our previous paper [5], the $3\,^1\Pi_u$ and $3\,^1\Sigma_u^+$ states are correlated with separated atoms $K(4\,^2S)+K(5\,^2P)$ and $K(4\,^2S)+K(3\,^2D)$, respectively. The dissociation energy of the $X\,^1\Sigma_g^+$ ground state, corresponding to the atomic configuration $K(4\,^2S)+K(4\,^2S)$, was reported as 4451 cm^{-1} [16]. Making use of the atomic energy-level spacings $\delta E(5\,^2P\text{-}4\,^2S)=24\,711$ cm^{-1} and $\delta E(3\,^2D\text{-}4\,^2S)=21\,536$ cm^{-1} [17], the dissociation energies of both excited states can be obtained from the relation

$$\mathcal{D}_e(3\,^1\Pi_u,3\,^1\Sigma_u^+)=\mathcal{D}_e(X\,^1\Sigma_g^+)+\delta E-T_e(3\,^1\Pi_u,3\,^1\Sigma_u^+)\,.$$

This yields $\mathcal{D}_e(3\,^1\Pi_u)=5175$ cm^{-1} and $\mathcal{D}_e(3\,^1\Sigma_u^+)=2314$ cm^{-1}. Consequently, the Dunham coefficients listed in Tables II and III describe the $3\,^1\Pi_u$ state to about 55% and the $3\,^1\Sigma_u^+$ state to 71% of their potential well depths. For the $3\,^1\Pi_u$ state a small value of Y_{00} [11], equal to -0.02 cm^{-1}, proves the consistency of the constants obtained. (Note that in Tables II and III Y_{00} is incorporated into T_e.) Also the experimental Y_{02} and Y_{11} coefficients compare favorably with those calculated using the Kratzer and Pekeris relations [11] ($Y_{02}=-0.667\times10^{-7}$ cm^{-1}, $Y_{11}=-0.314\times10^{-3}$ cm^{-1}), indicating that the $3\,^1\Pi_u$ state is well behaved and should be well approximated by a Morse potential curve. The $3\,^1\Sigma_u^+$ state is less regular. In trying to fit its term values,

TABLE II. Molecular constants for the $3\,^1\Pi_u$ state of $^{39}K_2$ (in cm^{-1}, except for R_e). The number in brackets that follows a quantity is the exponent of 10 that multiplies the quantity. The quoted error σ of a constant is one standard deviation. rms stands for the root-mean-square deviation of the fit.

Constant	This work Value	σ (%)	Theoretical Ref. [19]
T_e	23 987.1406	0.0002	23 500
Y_{10}	0.625 564[2]	0.018	
Y_{20}	−0.367 428[0]	0.294	
Y_{30}	0.694 778[−2]	0.731	
Y_{40}	−0.820 809[−4]	1.337	
Y_{50}	0.364 593[−6]	2.352	
Y_{01}	0.402 625[−1]	0.024	
Y_{11}	−0.260 580[−3]	0.522	
Y_{21}	0.369 527[−5]	1.880	
Y_{31}	−0.318 404[−7]	3.247	
Y_{02}	−0.633 647[−7]	0.776	
y_{01}	−0.849 838[−4]	1.431	
$\mathcal{D}_e$	5175		5659
R_e (Å)	4.636	0.022	4.46
No. of lines fitted	646		
rms	0.078		

TABLE III. Molecular constants for the $3\,^1\Sigma_u^+$ state of $^{39}K_2$ (presented as in Table II).

Constant	This work value	σ (%)	Theoretical Ref. [18]	Ref. [19]
T_e	23 672.8272	0.001	23 283	23 120
Y_{10}	0.658 830[2]	0.077	55.06	
Y_{20}	−0.618 231[0]	0.976		
Y_{30}	0.181 236[−1]	2.294		
Y_{40}	−0.498 417[−3]	3.012		
Y_{50}	0.248 298[−5]	8.443		
Y_{01}	0.390 092[−1]	0.182		
Y_{11}	−0.981 818[−4]	16.838		
Y_{21}	−0.172 259[−4]	8.912		
Y_{31}	0.946 015[−6]	6.650		
Y_{41}	−0.217 907[−7]	4.279		
Y_{02}	−0.914 088[−7]	5.247		
Y_{12}	0.631 151[−8]	9.744		
Y_{22}	−0.322 913[−9]	5.510		
$\mathcal{D}_e$	2314		2697	2870
R_e (Å)	7.410	0.085	5.024	4.56
No. of lines fitted	282			
rms	0.093			

TABLE IV. Rotationless RKR potential for the $3\,^1\Pi_u$ state of K_2. The first line refers to the bottom of the potential curve: r is the equilibrium distance.

v	V (cm^{-1})	r_{min} (Å)	r_{max} (Å)
	0.0	4.6359	
0	31.193	4.4772	4.8107
1	93.037	4.3697	4.9500
2	154.206	4.2993	5.0519
3	214.738	4.2442	5.1385
4	274.669	4.1979	5.2161
6	392.864	4.1213	5.3547
8	509.043	4.0584	5.4789
10	623.431	4.0043	5.5934
12	736.227	3.9565	5.7008
14	847.608	3.9135	5.8024
16	957.726	3.8743	5.8994
18	1066.713	3.8383	5.9924
20	1174.679	3.8048	6.0820
22	1281.719	3.7735	6.1686
24	1387.908	3.7441	6.2526
26	1493.305	3.7164	6.3342
28	1597.957	3.6901	6.4138
30	1701.895	3.6652	6.4916
32	1805.142	3.6413	6.5678
34	1907.707	3.6186	6.6426
36	2009.593	3.5967	6.7163
38	2110.795	3.5757	6.7891
40	2211.302	3.5556	6.8610
42	2311.097	3.5362	6.9323
44	2410.163	3.5175	7.0031
46	2508.477	3.4995	7.0737
48	2606.019	3.4822	7.1440
50	2702.770	3.4656	7.2142
52	2798.710	3.4497	7.2845
53	2846.372	3.4420	7.3197

the number of constants required for describing the measurements had to be larger than that for the $3\,^1\Pi_u$ state. The calculated value of Y_{00} for this state is equal to -0.13 cm^{-1} and differences of the fitted Y_{02} and Y_{11} constants from the Kratzer and Perkeris values reach up to 75%. At this stage we are not able to distinguish whether this reflects the fact that we fitted levels ranging from the lowest one up to only 670 cm^{-1} below the dissociation limit or that the potential curve of the $3\,^1\Sigma_u^+$ state is distorted by interaction with some other electronic state.

Once the coefficients in the Dunham expansion have been determined, we applied the Rydberg-Klein-Rees (RKR) method to obtain the rotationless potential curves for the $3\,^1\Pi_u$ and $3\,^1\Sigma_u^+$ states. The RKR curves, together with the vibrational term values $G(v)$, are given in Tables IV and V. It is interesting to compare the experimentally obtained parameters of the $3\,^1\Pi_u$ and $3\,^1\Sigma_u^+$ state potential curves with those calculated theoretically. The medium-excited states of K_2 have been the subject of various pseudopotential calculations [18,19] (see Tables II

TABLE V. Rotationless RKR potential for the $3\,^1\Sigma_u^+$ state of K_2.

v	V (cm^{-1})	r_{min} (Å)	r_{max} (Å)
	0.0	4.7098	
0	32.796	4.5520	4.8775
1	97.499	4.4416	5.0094
2	161.114	4.3682	5.1063
3	223.727	4.3104	5.1895
4	285.412	4.2619	5.2650
5	346.233	4.2199	5.3354
6	406.241	4.1827	5.4022
7	465.480	4.1491	5.4663
8	523.982	4.1186	5.5283
9	581.770	4.0906	5.5887
10	638.856	4.0646	5.6477
11	695.244	4.0403	5.7057
12	750.931	4.0175	5.7630
13	805.902	3.9960	5.8196
14	860.136	3.9756	5.8760
15	913.604	3.9562	5.9323
16	966.268	3.9377	5.9887
17	1018.084	3.9199	6.0456
18	1069.001	3.9029	6.1031
19	1118.959	3.8865	6.1617
20	1167.896	3.8709	6.2217
21	1215.738	3.8559	6.2834
22	1262.411	3.8415	6.3473
23	1307.831	3.8279	6.4138
24	1351.911	3.8151	6.4836
25	1394.558	3.8032	6.5571
26	1435.676	3.7921	6.6352
27	1475.163	3.7821	6.7187
28	1512.913	3.7733	6.8085
29	1548.817	3.7659	6.9060
30	1582.762	3.7599	7.0125
31	1614.632	3.7557	7.1299
32	1644.308	3.7534	7.2605

and III). Jeung and Ross [18] give molecular constants only for the $3\,^1\Sigma_u^+$ state: their potential curve is too deep by about 400 cm^{-1} and their equilibrium position some 0.3 Å too large. Duda [19] has calculated potential curves of both $3\,^1\Pi_u$ and $3\,^1\Sigma_u^+$ states. He also overestimates the well depths (by about 475 and 490 cm^{-1}, respectively) and his equilibrium distances are consistently too low. However, the relative positions of both curves are represented quite well: the bottom of the potential well of the $3\,^1\Sigma_u^+$ state is lower by 380 cm^{-1} than that of the $3\,^1\Pi_u$ state (vs the experimental value 314 cm^{-1}) and the equilibrium distance shifted by 0.10 Å towards larger R (experimentally 0.074 Å). This shows that pseudopotential calculations are capable of predicting the properties of medium-excited electronic states of small molecules with acceptable accuracy, but experimental data are still superior in this field.

ACKNOWLEDGMENT

This research was supported by the Polish Committee for Scientific Research (Grant KBN No. 2 2332 92 03).

[1] S. Magnier, Ph. Millié, O. Dulieu, and F. Masnou-Seeuws, J. Chem. Phys. **98**, 7113 (1993), and references therein.

[2] A. R. Rajaei-Rizi, F. B. Orth, J. T. Bahns, and W. C. Stwalley, J. Mol. Spectrosc. **109**, 123 (1985); C. Linton, R. Bacis, P. Crozet, F. Martin, A. J. Ross, and J. Vergès, J. Phys. IV (France) Colloq. **52**, C7-505 (1991); W. H. Jeng, X. Xie, L. P. Gold, and R. A. Bernheim, J. Chem. Phys. **94**, 928 (1991), and references therein.

[3] T. J. Whang, W. C. Stwalley, L. Li, and A. M. Lyyra, J. Mol. Spectrosc. **155**, 184 (1992), and references therein.

[4] H. Wang, W. C. Stwalley, and A. M. Lyyra, J. Chem. Phys. **96**, 7965 (1992), and references therein.

[5] W. Jastrzębski and P. Kowalczyk, Chem. Phys. Lett. **206**, 69 (1993).

[6] N. W. Carlson, A. J. Taylor, K. M. Jones, and A. L. Schawlow, Phys. Rev. A **24**, 822 (1981).

[7] Z. G. Wang and H. R. Xia, *Molecular and Laser Spectroscopy* (Springer, Berlin, 1991).

[8] A. R. Striganov and G. A. Odincova, *Tablicy Spektralnych Linii Atomov i Ionov* (Energoizdat, Moscow, 1982).

[9] A. N. Nesmeyanov, *Vapour Pressure of the Elements* (Elsevier, London, 1963).

[10] W. Jastrzębski, P. Kowalczyk, and R. Ferber (unpublished).

[11] G. Herzberg, *Molecular Spectra and Molecular Structure.* Vol. I. Spectra of Diatomic Molecules (Van Nostrand–Reinhold, Princeton, NJ, 1950).

[12] A. J. Ross, P. Crozet, J.d'Incan, and C. Effantin, J. Phys. B **19**, L145 (1986).

[13] P. Kowalczyk, A. Katern, and F. Engelke (unpublished results).

[14] A. Katern, Ph.D. thesis, Bielefeld Universität, 1988.

[15] P. Kowalczyk, A. Katern, and F. Engelke, Z. Phys. D **17**, 47 (1990).

[16] C. Amiot, J. Mol. Spectrosc. **147**, 370 (1991).

[17] A. A. Radzig and P. M. Smirnov, *Reference Data on Atoms, Molecules and Ions* (Springer, Berlin, 1985).

[18] G. H. Jeung and A. J. Ross, J. Phys. B **21**, 1473 (1988).

[19] C. A. Duda, M.Sc. thesis, State University of New York at Binghamton, 1986.